ACS APPLIED MATERIALS & INTERFACES

Research Article

www.acsami.org

Breakdown and Protection of ALD Moisture Barrier Thin Films

Frederik Nehm,*[,†] Hannes Klumbies,[†] Claudia Richter,[‡] Aarti Singh,[‡] Uwe Schroeder,[‡] Thomas Mikolajick,[‡] Tobias Mönch,[†] Christoph Hoßbach,[§] Matthias Albert,[§] Johann W. Bartha,[§] Karl Leo,[†] and Lars Müller-Meskamp[†]

[†]Institut für Angewandte Photophysik, Technische Universität Dresden, 01062 Dresden, Germany

[‡]NaMLab gGmbH, Nöthnitzer Straße 64, 01187 Dresden, Germany

[§]Institut für Halbleiter und Mikrosystemtechnik, Technische Universität Dresden, 01062 Dresden, Germany

ABSTRACT: The water vapor barrier properties of low-temperature atomic layer deposited (ALD) AlO_x thin-films are observed to be unstable if exposed directly to high or even ambient relative humidities. Upon exposure to humid atmospheres, their apparent barrier breaks down and their water vapor transmission rates (WVTR), measured by electrical calcium tests, deteriorate by several orders of magnitude. These changes are accompanied by surface roughening beyond the original thickness, observed by atomic force microscopy. X-ray reflectivity investigations show a strong decrease in density caused by only 5 min storage in a 38 °C, 90% relative humidity climate. We show that barrier stabilities required for device applications can be achieved by protection layers which prevent the direct contact of water condensing on the surface, i.e., the sensitive ALD barrier. Nine different protection layers of either ALD materials or polymers are tested on the barriers. Although ALD materials prove to be ineffective, applied polymers seem to provide good protection independent of thickness, surface free energy, and deposition technique. A glued-on PET foil stands out as a low-cost, easily processed, and especially stable solution. This way, 20 nm single layer ALD barriers for organic electronics are measured. They yield reliable WVTRs down to 2×10^{-5} g(H_2O) m^{-2} day^{-1} at 38 °C and 90% relative humidity, highlighting the great potential of ALD encapsulation.

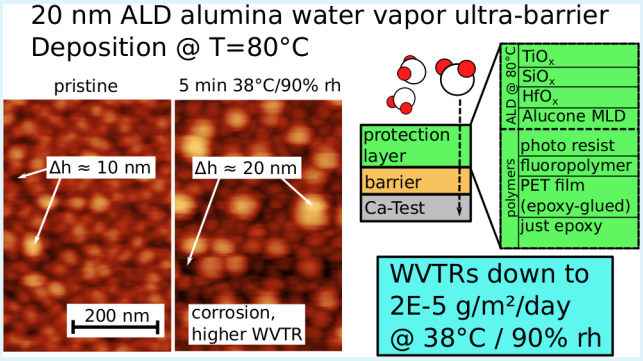

KEYWORDS: *water vapor, barrier, encapsulation, atomic layer deposition, corrosion, WVTR*

INTRODUCTION

In recent years, the demand for ultrahigh water vapor barriers has drastically increased because of the continuous progress of organic devices.[1,2] Highly efficient organic solar cells and organic light-emitting diodes can only achieve mass production if certain product lifetimes are reached with affordable encapsulation systems. Estimations and measurements show that reasonable lifetimes of more than 5 years require water vapor transmission rates (WVTRs) of a complete encapsulation between 1×10^{-5} and 1×10^{-6} g(H_2O) m^{-2} day^{-1}.[3,4] This is roughly equivalent to a monolayer of water permeating into the device in a month or a year, respectively.

Atomic layer deposited (ALD) thin films of materials like AlO_x have emerged in recent years as a reliable source for ultrahigh barriers bcause of their nearly defect-free nature and conformal deposition. High barrier performance has been reported for such films, regardless of deposition on polymer sheets or as thin-film device encapsulation. WVTRs down to the 1×10^{-6} g(H_2O) m^{-2} day^{-1}regime have been stated in literature, although processes, measurements, and conditions are often not well comparable.[5−7] Nonoptimal processing parameters or handling can easily lead to barrier shortcomings. Macro defects—so-called pinholes—are a major issue for barrier production, leading to the well-known dark spot formation in organic light-emitting diodes. Another type of failure, a barrier malfunction, can hinder a correct barrier quality assessment. In the case of a malfunction, water ingress can suddenly and dramatically overshoot expectations for the barrier material in question. A possible explanation for this behavior can be the corrosion of the ALD AlO_x films, as shown before.[8−11] A crucial point further aggravating the matter are the low ALD process temperatures limited to around 100 °C required when depositing onto organic devices, i.e., thin-film encapsulation. For such low-temperature processes, Carcia et al. have proposed the incorporation of hydroxide in the aluminum oxide matrix, which renders the emerging films vulnerable to corrosion in contact with water.[9]

Several coatings providing sufficient corrosion protection for ALD layers have been reported. For AlO_x grown on Cu, Abdulagatov et al.[10] showed that a layer of ALD-deposited TiO_2 stabilizes the film. Kim et al.[11] successfully applied parylene as protective film to impede condensation directly on

Received: December 5, 2014
Accepted: September 24, 2015
Published: September 24, 2015

DOI: 10.1021/acsami.5b06891
ACS Appl. Mater. Interfaces 2015, 7, 22121−22127

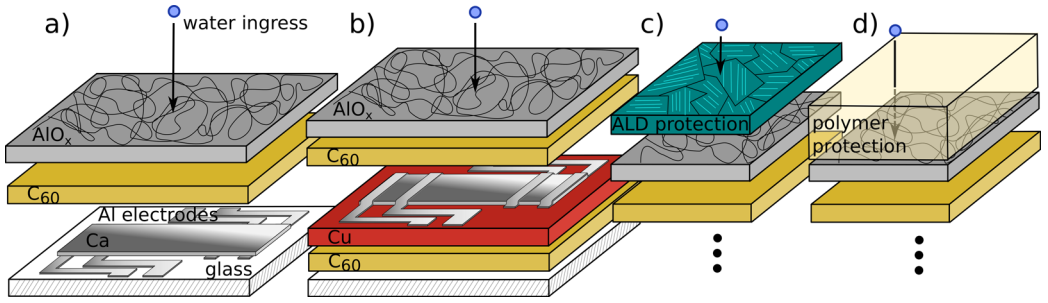

Figure 1. Schematics for used Ca-Tests and barrier protection strategies. (a) Ca-Test layout A, (b) Ca-Test layout B, (c) ALD thin-film protection, (d) polymer film protection.

the barrier. For thin-film encapsulation, rapid-ALD-deposited silica,[8] 100 nm PECVD-deposited SiN,[11] and 25 nm ALD-deposited titania were reported to protect the ALD layer.[10] However, a comparative investigation on different protective layers is still lacking.

A complete evaluation of device encapsulation requires its application on a device and measurement of its functionality over time. This technique yields reliable lifetime values, but it is slow, expensive, and specific for the device in question. Measuring WVTRs directly is faster, cheaper, yields additional information on the barrier, and the gained information can directly be related to device lifetimes as well. A sensitive and cost-efficient method to measure WVTRs reliably down to at least 1×10^{-5} g(H_2O) m^{-2} day^{-1} is the electrical calcium corrosion test (Ca-Test).[12−14] It monitors the conductivity decrease of a thin calcium film turning into calcium hydroxide due to contact with water. The measured WVTRs can be roughly related to device lifetimes.[4] To allow a valid relation between permeation barrier and device lifetime, we have to use a setup close to an actual device layout and design, as it is selected for this study. Climatic test conditions are to be chosen carefully as well, since WVTRs are dependent on both humidity and temperature. Especially high relative humidity, a condition unavoidable in outdoor use, can drastically accelerate degradation.

In this work, we show evidence for corrosion of ALD AlO_x with X-ray reflectivity (XRR) and atomic force microscopy (AFM) measurements. We then present ways to circumvent barrier failure due to corrosion. We observe that covering an atomic layer deposited (ALD) amorphous alumina barrier proves to be crucial to prevent corrosion. We show that other ALD materials like SiO_x, HfO_x, and TiO_x can act as protection layer, however, are ultimately insufficient if processed at device-friendly conditions below 100 °C. On the other hand, several different polymer layers—independent of thickness, surface free energy, and deposition technique—provide sufficient protection capability. As a solution, we propose a glued-on polymer foil (such as PET) to inhibit corrosion of the barrier film. This way, a stable Ca-Test can be performed which allows for a measurement of excellent barrier quality. WVTRs of $(2-3) \times 10^{-5}$ g(H_2O) m^{-2} day^{-1} are confirmed for 20 nm single layer barriers measured at 38 °C and 90% relative humidity, highlighting the great potential of ALD ultrabarriers with additional protection layers.

EXPERIMENTAL SECTION

In this work, thin films of low-temperature ALD AlO_x are studied as water vapor barriers on electrical calcium corrosion tests to evaluate barrier quality in respect to the encapsulation of organic electronic devices. To prevent an observed barrier malfunction, we investigated different cover materials for sufficient protection of the underlying AlO_x barrier from corrosion. For barrier quality assessment, water vapor transmission rates are measured with electrical calcium corrosion tests, which use the change in conductance of an evaporated metallic Ca stripe turning into calcium hydroxide over time. This reaction occurs when Ca is brought in contact with water, which in our case is permeating through the ALD barrier. The climate conditions throughout the permeation measurement are kept constant at 38 °C and 90% relative humidity (RH). For further details regarding the setup, see12. Two architectures for the thin-film design of the Ca-Test were used in this investigation, which from now on are referred to as layout A and layout B, both of which can be seen in Figure 1. Essentially, layout B presents a newer version of the test, which works with higher stability and sensitivity. However, results from both tests are shown for better understanding of the investigation. In both test layouts, correct conductance values are guaranteed by a 4-wire-sense layout of the electrodes that measure the calcium corrosion without a series resistance.[15] Also, C_{60} is used for mechanical decoupling of the barrier and the Ca sensor.[16] This proves necessary because of Ca expansion during corrosion. In layout A, the thickness of the mechanical decoupling is chosen too thin compared to the Ca sensor. This leads to a mechanical breakdown of the barrier and subsequent abrupt test failure after a certain level of water ingress. Using layout A, no valid WVTRs can be measured. Instead the time until a rapid conductance loss leads to a complete test failure is used as a measure of quality of the protection. Layout B of the Ca-Test uses a second mechanical decoupling layer below a thinner Ca sensor for stress mitigation.[17] Additionally, a 25 nm thin Cu layer prohibits a corrosion element to form between the Al contacts and the Ca sensor, which leads to a bottleneck degradation.[18] As the conductivity of the Cu layer is constant during the measurement and the WVTR is dependent on the test's derivative of the conductivity, the Cu layer itself does not contribute to the WVTR. The following layers are thermally evaporated in vacuum for layout A: Al contacts (100 nm), Ca sensor (100 nm), 100 nm C_{60}. Layout B uses the following layers: 100 nm C_{60}, 25 nm Cu, 60 nm Ca sensor, 100 nm Al contacts, 150 nm C_{60}. Afterward, the ALD barrier and ALD or polymer protection layer are deposited. All comparative barrier film calcium tests are processed on 125 μm planarised Teonex PEN (DupontTeijin, Tokyo, Japan). The AlO_x barrier is deposited first, followed by 20 nm of C_{60} decoupling layer, 100 nm of Ca sensor, and 100 nm Al 4-wire electrodes. The deposition side of the foil is afterward sealed with an encapsulation glass, which has a nitrogen-filled cavity facing the Ca sensor. Thus, only the rim is glued on with UV-curing XNR 5590 (Nagase ChemteX Corporation, Shinmachi, Nishi-Ku, Osaka, Japan). Material evaporation for the calcium tests takes place in a custom-made high vacuum chamber (K. J. Lesker Company, Clairton, Pennsylvania, USA) at a pressure of approximately 1×10^{-7} mbar, where all required layers can be processed without breaking the vacuum in between. Application of a sample layout is done by different shadow masks in the evaporation path. The evaporation system is connected to a glovebox (MBraun, Garching, Germany) with nitrogen atmosphere. This enables sample preparation under inert conditions with a residual amount of water and oxygen below 1 ppm.

DOI: 10.1021/acsami.5b06891
ACS Appl. Mater. Interfaces 2015, 7, 22121−22127

Additionally, solitary barrier layers, deposited directly on glass substrates with just an organic layer below for comparable ALD growth, are used to investigate barrier corrosion in contact with humidity. AFM images and X-ray reflectivity measurements are made for this purpose. AlO_x barriers with calcium tests underneath are covered with four different ALD materials (TiO_x, HfO_x, SiO_x, and Alucone) and four different polymers (NOVEC EGC-1700, nLOF 2020, PET, and UV-curing epoxy), see Figure 1 for schematics. AlO_x, TiO_x, and Alucone layers are deposited in a Beneq TFS 500 ALD system. Handling is possible under completely inert conditions due to an attached glovebox with residual water and oxygen amounts below 0.1 ppm. HfO_x and SiO_x layers are deposited in an Oxford OpAL Plasma ALD.

The following precursors are used for the ALD layers investigated: Electronic grade trimethylaluminum (TMA) and ozone for AlO_x, electronic grade titanium tetrachloride and deionized water (quality according to VDI standard 2083) for TiO_2, Tetrakis-[EthylMethylAmino] Hafnium (TEMAHf, Air Liquide, Paris, France) and deionized water for HfO_2, SilaneDiAmine, *N,N,N′,N′*-TetraEthyl (SAM.24, Air Liquide, Paris, France) and O_2 plasma for SiO_2, TMA and mono ethylene glycol (anhydrous, 99.8% purity) for aluminum alkoxide (Alucone). Nitrogen gas with 99.9999% chemical purity is used for chamber purging between precursor feeds. For HfO_2 and SiO_2 deposition, argon gas with 99.999% purity is used for chamber purging. All ALD films are processed at 80 °C. However, to draw a comparison to the barriers resulting from a less device-friendly ALD process, neat alumina films are also deposited at 100 °C using plasma enhanced ALD in a Sentech SI reactor (SENTECH Instruments GmbH, Berlin, Germany) with glovebox integration.

Materials used for polymer protection layers are spin-coated 3 M (St. Paul, Minnesota, USA) NOVEC EGC-1700 (2% in HFE 7100, spun at 1500 and 3000 rpm), spin-coated (3000 rpm) negative photo resist nLOF 2020 (AZ^R Electronic Materials, Luxembourg City, Luxembourg), 125 μm DupontTeijin (Tokyo, Japan) Melinex ST504 PET sheets, glued-on with UV-curing epoxy XNR 5590 (Nagase ChemteX Corporation, Shinmachi, Nishi-Ku, Osaka, Japan), and XNR 5590 without PET foil. Thicknesses of the polymer protection layers are identified using a Profilometer. Surface free energies of all protection layers, as well as the neat alumina films are ascertained using ACCU DYNE TEST marker pens (Diversified Enterprises, Claremont, NH, USA) with detection values from 30−60 dyn/cm.

All thin-film encapsulation calcium tests as well as AFM and XRR samples are produced on 1 by 1 in. glass substrates (BK7, Schott, Mainz, Germany).

For AFM and XRR samples, first 100 nm of C_{60} are deposited in vacuum by thermal evaporation onto the substrate. This step ensures comparable ALD growth behavior to organic devices as well as the Ca-tests. Afterward 20 nm AlO_x are grown in a low-temperature ALD process.

For AFM measurements, a sample is inserted into a special AFM stage within a glovebox. The stage itself is then sealed with a latex membrane, keeping the sample in the inert and water-free glovebox atmosphere. This setup was described in detail by Klumbies et al.[19] In a plastic transport container, the sample is then moved from the glovebox to the AFM. With opening the transport container, water vapor slowly starts entering the sample atmosphere through the latex membrane until equilibrium is reached with the ambient air. Stage insertion is done directly after transport and images are taken as soon as possible, approximately 5−10 min after stage exposure to atmosphere. Images are taken with an AIST-NT Combiscope (Novato, California, USA) in tapping mode. Tips used are TAP-Al-G by BudgetSensors with a resonance frequency of approximately 320 kHz.

RESULTS AND DISCUSSION

In this section, we present evidence for the corrosion of AlO_x ALD films upon direct exposure to humidity and subsequent failure of the barrier. To make the barrier films feasible for later device encapsulation, protective methods against barrier malfunction are then discussed and subsequently evaluated.

When studying the performance of low-temperature atomic layer deposited alumina as thin-film barriers for the encapsulation of organic electronic devices, we note an unusual behavior of Ca-tests with layout A (see Experimental Section), employed for the barrier measurement. The test current (which decreases proportionally to the humidity ingress) behaves highly nonlinear, if the ALD film is exposed directly to humidity (see Figure 2). Ideally, electrical calcium test data

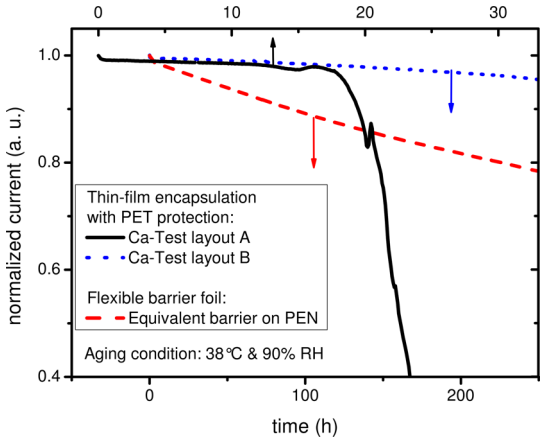

Figure 2. Normalized current traces over time for three Ca-Tests measuring equal 20 nm AlO_x barriers. Dashed line, Ca test on barrier and polymer film; solid line, thin-film encapsulation with glued-on PET for Ca-Test layout A; dotted line, thin-film encapsulation with glued-on PET for Ca-Test layout B.

(current through the calcium vs time) shows a linear decrease of current over time once permeation in the test reaches steady-state. When performing an electrical calcium test (layout A) with a thin-film ALD encapsulation, that faces a high relative humidity air volume, the conductance of the calcium decreases rapidly in a matter of minutes after exposure. Equivalent barriers processed on polymer sheets with Ca-tests deposited directly on the barrier allow weeks of Ca-Test measurement with WVTRs in the regime of 10^{-4} g(H_2O) m^{-2} day^{-1} at 38 °C and 90% RH. However, in this case, the barrier film resides on the dry side of the test and the polymer substrate faces the outside humidity. Exemplary conductance traces for both measurement types are depicted in Figure 2.

Both types of barrier measurements are of interest for organic device encapsulation. The first type of measurement with the barrier thin-film facing the atmosphere corresponds to a thin-film encapsulation approach, where a barrier is processed directly on a device to prevent side diffusion issues. The second type of measurement with the barrier film on a polymer substrate corresponds to premanufactured barrier foils that can be used as substrates or laminated onto a device—the barrier facing inward.

To investigate the underlying cause for the barrier malfunction, we recorded AFM images of the solitary barrier films in nonaged condition, during slow humidity increase to ambient (see Experimental Section for details), and again after 5 min of exposure to a 38 °C and 90% relative humidity (RH) climate. The extracted root-mean-square (RMS) roughness from these images shows a slow increase over time during 1 day of increasing humidity to ambient. Roughness values of nonaged layers start at 1.1 nm and seem to saturate at 1.8

DOI: 10.1021/acsami.5b06891
ACS Appl. Mater. Interfaces 2015, 7, 22121−22127

nm after ambient aging. After only 5 min of exposure to 90% relative humidity, the measured roughness is 3.7 nm, an increase of more than 100% compared to ambient aging. Figure 3 shows the AFM images of the nonaged and completely aged

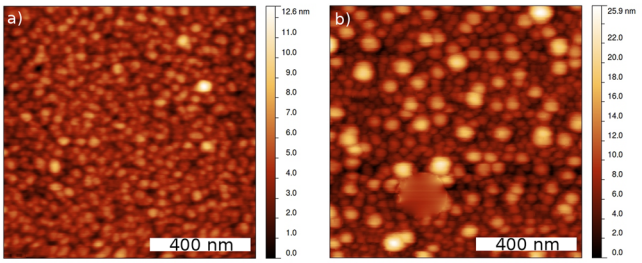

Figure 3. AFM images of (a) as-deposited (nonaged) low-temperature ALD AlO_x film and (b) after 5 min of aging in 38 °C and 90% RH atmosphere. Hillock formation and strong roughness increase are observed.

films. It reveals the nature of the roughening in a development of hillocks both higher and larger in diameter than typical surface features.

Note that the surface features of the aged sample measure over 20 nm from lowest to highest peak, which is in the range of the nominal barrier film thickness, suggesting serious changes in the microstructure of the thin-film.

For further investigation, XRR measurements are performed on pristine (nonaged) barrier films as well as on samples aged at 38 °C and 90% RH for 5, 15, and 60 min. Fits of the data reveal a decrease in material density with increasing exposure, while the film thickness remains roughly constant as can be seen in Figure 4. The AlO_x density of the ALD thin film starts

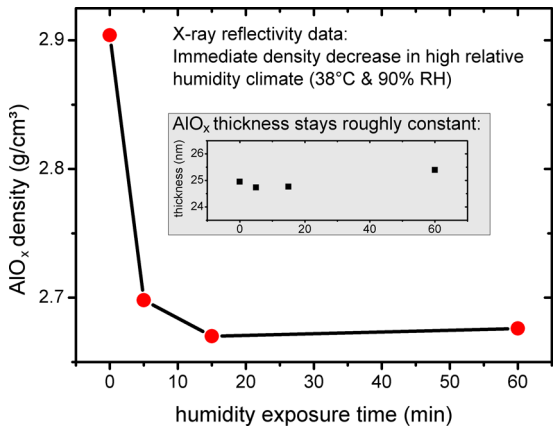

Figure 4. XRR density of the AlO_x films after 0, 5, 15, and 60 min of aging in 38 °C and 90% RH climate. ALD was carried out on a glass substrate with 100 nm of evaporated C_{60}. The density drops after only 5 min and saturates. It does not change significantly with further aging. Inset: The XRR thickness of the films stays roughly constant over aging time.

out at approximately 2.9 g/cm^3 for pristine layers and drops to around 2.7 g/cm^3 for the sample exposed to only 5 min of aging. For samples exposed to further aging, the density remains at this low value. From the observed barrier malfunction in the Ca test, the surface roughness increase measured by AFM and the density loss detected by XRR suggest a restructuring of the AlO_x thin film. These effects are likely to cause pinholes, cracks, and low density areas, which are open for increased water permeation.

Crystalline alumina exhibits a density of 3.965 g/cm^3 [20] and was shown in literature to withstand the aging conditions (38 °C, 90% RH) shown in this publication.[21] As the ALD barriers used here are intended to be processed directly onto devices and polymer foils, the deposition temperatures are limited and were chosen as 80 °C. For such conditions, ALD AlO_x films were shown not to be crystalline but amorphous with densities at approximately 2.8−2.9 g/cm^3.[22,23] Both AFM and XRR data show a change in morphology and density of the barrier layers after aging. Hydroxide groups left from incomplete TMA reactions are expected to promote water incorporation and thus, rearrangement and degradation of the barrier. As reasoned by Carcia et al., the lower density is directly connected to a high hydrogen content within the film and is not uncommon for low-temperature ALD films.[9] Carbon residue, also known to be present in low-temperature alumina ALD films,[24] could contribute as well to water incorporation. We assume that interaction of the thin film with water condensed from the humid atmosphere is responsible for hillock formation and roughness increase on the AFM images and density decrease in the XRR data. This leads to rapid failure of the barrier and breakdown of the calcium corrosion test beneath the barrier. After 5 min of exposure, further changes in AFM images and XRR data can not be observed, highlighting the fast pace of the barrier corrosion in the high humidity environment (38 °C and 90% RH).

In order to inhibit the observed barrier corrosion of the ALD thin-films, different protection layers are deposited onto the thin-film barriers and evaluated using electrical calcium corrosion tests (Ca-Tests). The protection layers can roughly be divided into two material classes: ALD protection layers and polymer protection layers. The corresponding Ca-test schematics are depicted in Figure 1. Our selection of ALD materials for the protective layer is motivated by successful application in literature (see Introduction) and ease of processing in the same deposition chamber as the barrier. The selected ALD materials are expected to exhibit lower susceptibility to corrosion due to different properties like higher density or crystallinity as well as less hydrogen and carbon incorporation. Polymers on the other hand, impede direct condensation of water vapor on the ALD film, thereby completely changing the type of exposure. As protection layers 10 nm silicon oxide (SiO_2), 10 nm titanium oxide (TiO_2), 10 nm hafnium oxide (HfO_2), 10 nm aluminum alkoxide (Alucone), and a glued-on Melinex^R PET sheet (see Experimental Section for details) are selected for layout A of the Ca-Test, which exhibits a breakdown. As discussed shortly in the Experimental Section, this breakdown is caused by an inter-relation of barrier corrosion and barrier cracking because of Ca expansion.[16] In case of the thin-film encapsulation Ca-Test with layout A, this mechanism creates a self-accelerating effect. The more water permeates through the barrier, the faster the calcium expands, cracking the barrier and causing it to fail. This procedure can be observed as a strongly decreasing Ca-Test current slope (and thus rising apparent WVTR) until all Ca is corroded—a Ca-Test breakdown. The investigation is repeated with Ca-Test layout B, which offers better sensitivity and stability without the risk of a breakdown. Here, the materials chosen for corrosion protection are TiO_x to represent low-temperature ALD materials and the following polymers: spin-coated EGC-1700 (at 3000 and 1500 rpm), spin-coated

DOI: 10.1021/acsami.5b06891
ACS Appl. Mater. Interfaces 2015, 7, 22121−22127

negative photo resist nLOF 2020 (at 3000 rpm), a Melinex[R] PET sheet glued-on with UV-curing epoxy XNR 5590, and XNR 5590 without a PET sheet.

Although, using Ca-Test layout A, the tests exhibit a breakdown with every protection layer, a clear trend can be observed in the time until a breakdown occurs. This time can be interpreted as a rough estimate of the protection capability. A better protection leads to a slower or postponed barrier restructuring. It thus takes longer for a certain amount of water to enter the test. As discussed above, a breakdown occurs due to an expansion of the calcium during corrosion after enough water has ingressed through the barrier. A postponed entry of a certain water amount thus leads to a postponed breakdown. Table 1 shows the times until breakdown for Ca-Test layout A.

Table 1. Protective Capabilities of Five Different Materials Covering 20 nm of Low-Temperature ALD Alumina[a]

protection layer (on Ca-Test layout A)	time until breakdown
nothing	approximately 3 min
10 nm SiO_x (thermal ALD, 80 °C)	(5 ± 1) min
10 nm HfO_x (thermal ALD, 80 °C)	(15 ± 1) min
10 nm Alucone (thermal ALD, 80 °C)	(40 ± 11) min
10 nm TiO_x (thermal ALD, 80 °C)	(60 ± 10) min
125 μm PET (glued on with UV-curing epoxy)	(24 ± 3) h

[a]Measured in the time until a complete electrical breakdown of the tests is observed, using Ca-Test layout A. Three samples were processed for each condition.

We notice little to no effect for a SiO_x or HfO_x protection layer and Alucone postpones the breakdown for 40 min. As discussed in literature, out of the ALD layers, the most significant protective behavior is observed for a thin TiO_x film.[10,25] However, even this yields a breakdown time of only 1 h in our experiments. A glued-on PET film shows a breakdown after 24 h, which is a great improvement, compared to the protection layers from ALD. However, because the breakdown behavior in Ca-Test layout A arises from stress in the films, it is impossible to separate barrier and breakdown effects, which could be strongly influenced, for example, by the higher mechanical stress resistance of the thick, elastic polymer film cover. To complement the drastic observations on layout A, a more conclusive evaluation of the different protective capabilities is repeated with Ca-Test layout B, which does not suffer from breakdown behavior.

Figure 5 shows data on all protection layers investigated with Ca-Test layout B. These are the WVTRs of the Ca-Tests themselves, as well as thicknesses and surface free energies of the protection layers. Investigated layers are 10 nm TiO_x, representing the ALD protection layers, the fluoropolymer EGC-1700 spin-coated at two different spin speeds, spin-coated negative photo resist nLof 2020, 125 μm PET films glued on using UV-curing epoxy XNR 5590, and a pure layer of XNR 5590. In comparison, unprotected alumina barriers are shown. A breakdown can no longer be observed and WVTRs can be assessed for all samples. The unprotected low-temperature alumina exhibits a WVTR of 3×10^{-3} g(H_2O) m^{-2} day^{-1}. Just like for the Ca-Test layout A, ALD TiO_x shows a protective effect for the barrier, lowering the effective WVTR of the barrier by an order of magnitude to 3×10^{-4} g(H_2O) m^{-2} day^{-1}. We assume the other ALD materials used in Table 1 to influence the WVTR less effectively, since they all showed an earlier breakdown. Nonetheless, most ALD films tested as

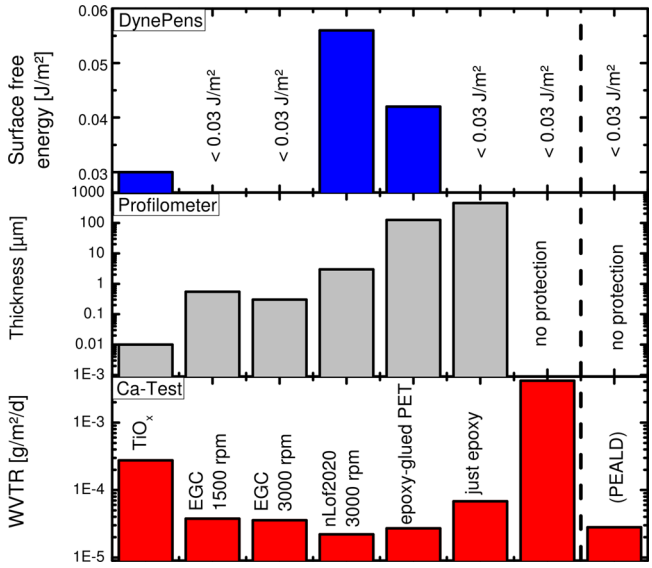

Figure 5. WVTRs, thickness, and surface free energy for all protection layers on 20 nm of ALD alumina. Also, two sample types are shown without protection layer: thermal ALD at 80 °C and plasma-enhanced ALD at 100 °C. Shown thickness data only accounts for the protection layer.

protection layers showed a corrosion inhibiting effect, which we attribute to a reduced susceptibility of the respective material to humidity upon adsorption and condensation at the surface.

Another order of magnitude is gained in the WVTR using the polymer protection layers. For almost all investigated polymer layers, we measure similar WVTRs of $2–4 \times 10^{-5}$ g(H_2O) m^{-2} day^{-1} in the Layout B configuration. A slightly higher WVTR of 7×10^{-5} g(H_2O) m^{-2} day^{-1} is observed for the UV-curing epoxy. The WVTRs seem unrelated to the thickness of the protection layer, their surface free energy, as well as the actual method of deposition, highlighting the importance of the sorption behavior. As long as a polymer coating is applied, the WVTR will be roughly constant and dominated by the ALD layer, likely because of the missing direct sorption taking place on the barrier surface. Thus, the results from layout B confirm the necessity of barrier protection and the benefit of polymer protection films observed for test layout A.

The poor performance of the additional low-temperature ALD protection layers is likely caused by hydrogen or carbon incorporations as well as lacking crystallinity of the films. This might lead to a coarsening of the ALD protection layers themselves and subsequent partial exposure of the barrier to the outward air. For higher deposition temperatures, better protective capabilities can be expected, but those were avoided in the present work to keep the results applicable to actual organic devices. The benefits of a less device-friendly barrier deposition can be seen in Figure 5: For a direct comparison, a neat 20 nm barrier layer of AlO_x is deposited at a higher temperature of 100 °C and using atomic oxygen from a plasma source as second precursor. The barrier deposited this way exhibits a WVTR of 3×10^{-5} g(H_2O) m^{-2} day^{-1} without any protection layer, strongly suggesting that little or no barrier corrosion is taking place. However, many organic devices cannot withstand such deposition conditions and thus such a barrier cannot be generally recommended for thin-film encapsulation.

DOI: 10.1021/acsami.5b06891
ACS Appl. Mater. Interfaces 2015, 7, 22121–22127

The slightly higher WVTR for the epoxy protection layer can be explained by deposition details. Using the epoxy to glue on a PET film, only a small volume of epoxy is deposited with a needle onto the sample. Capillary forces spread this drop over the complete test area when the PET is laid onto it, reducing the epoxy thickness to a few microns. In case of a deposition of pure epoxy, this procedure cannot be used. A larger amount of epoxy has to be deposited that exhibits high variations in thickness. The measured WVTRs are well within the accuracy limit at such low detection rates for all other polymer protection layers. Out of those, the glued-on PET foil yields the most stable results (see Figure 2 for exemplary test data) and presents the easiest method described here. We wish to clarify that the intrinsic WVTR of a Melinex^{R} PET sheet (given by the manufacturer as 4 g m^{-2} day^{-1}) is at least 3 orders of magnitude higher than the WVTR of the measured AlO_x. The PET's influence on the barrier is thus not its own barrier performance but its ability to protect the AlO_x. The authors would like to recommend this simple technique for the protection of moisture barriers for lab experiments, as it has become a standard in-house procedure for the measurement of thin-film encapsulated calcium tests and devices due to its very good results and reliability. Since a basic mechanical protection will be needed for any market organic solar cell device, the usage of a polymer sheet for additional corrosion protection will be a synergetic effect and no extra effort.

CONCLUSION

We investigate the stability of low-temperature ALD alumina barrier thin-films deposited on C_{60}. Using electrical calcium corrosion test measurements, we observe strongly deteriorated barrier quality for the alumina layers directly exposed to humidity. With AFM and XRR measurements, we find a humidity-induced roughening of the films and a fast decrease in density which saturates after 5 min of exposure to 38 °C and 90% RH at most. We attribute these morphological changes to an incorporation of water and a microstructure rearrangement. Water incorporation and the subsequent failure of the barrier are likely caused by a high content of hydroxide groups within the films, a direct consequence of the low ALD process temperatures required for deposition on temperature-sensitive organic materials.

We successfully apply different protection layers to inhibit corrosion and barrier malfunction. Thin ALD protection layers of less humidity susceptible materials enhance the corrosion resistance and lower the measured WVTR by 1 order of magnitude for TiO_x. For a long-term ALD-barrier protection, however, all examined thin ALD protection-layers turn out to be ineffective. Comparable corrosion protection is achieved for all 5 tested polymer layers independent of thickness, surface free energy, and deposition technique. This way, for only 20 nm of low-temperature ALD AlO_x single-layer barriers, WVTRs of down to 2×10^{-5} g(H_2O) m^{-2} day^{-1} are measured at 38 °C and 90% RH. This highlights the sensitivity of high-barrier films and the importance of their surface or interfaces to the neighboring materials to achieve barriers with low and stable permeation. The investigation also emphasizes the immense potential of ALD barriers for the encapsulation of organic devices, which can withstand harsh climate conditions, even if processed at low temperatures.

AUTHOR INFORMATION

Corresponding Author

*E-mail: frederik.nehm@iapp.de.

Notes

The authors declare no competing financial interest.

ACKNOWLEDGMENTS

Financial support from the Bundesministerium für Bildung und Forschung (BMBF) within the Innoprofile Transfer project 03IPT602A is gratefully acknowledged. The authors thank Dr. Wilde for XRR measurements and Sven Kunze for maintenance of the measurement setup.

REFERENCES

(1) Heliatek Press Release. Heliatek Consolidates its Technology Leadership by Establishing a New World Record for Organic Solar Technology with a Cell Efficiency of 12%. http://www.heliatek.com/wp-content/uploads/2013/01/130116_PR_Heliatek_achieves_record_cell_effiency_for_OPV.pdf (accessed Nov 4, 2014).

(2) Sekine, C.; Tsubata, Y.; Yamada, T.; Kitano, M.; Doi, S. Recent Progress of High Performance Polymer OLED and OPV Materials for Organic Printed Electronics. *Sci. Technol. Adv. Mater.* **2014**, *15*, 034203.

(3) Burrows, P. E.; Graff, G. L.; Gross, M. E.; Martin, P. M.; Shi, M. K.; Hall, M.; Mast, E.; Bonham, C.; Bennett, W.; Sullivan, M. B. *Displays* **2001**, *22*, 65−69.

(4) Klumbies, H.; Karl, M.; Hermenau, M.; Rösch, R.; Seeland, M.; Hoppe, H.; Müller-Meskamp, L.; Leo, K. Water Ingress into and Climate Dependent Lifetime of Organic Photovoltaic Cells Investigated by Calcium Corrosion Tests. *Sol. Energy Mater. Sol. Cells* **2014**, *120*, 685−690.

(5) Carcia, P. F.; McLean, R. S.; Reilly, M. H.; Groner, M. D.; George, S. M. Ca Test of Al_2O_3 Gas Diffusion Barriers Grown by Atomic Layer Deposition on Polymers. *Appl. Phys. Lett.* **2006**, *89*, 031915.

(6) Langereis, E.; Creatore, M.; Heil, S. B. S.; van de Sanden, M. C. M.; Kessels, W. M. M. Plasma-Assisted Atomic Layer Deposition of Al_2O_3 Moisture Permeation Barriers on Polymers. *Appl. Phys. Lett.* **2006**, *89*, 081915.

(7) Singh, A.; Klumbies, H.; Schröder, U.; Müller-Meskamp, L.; Geidel, M.; Knaut, M.; Hoßbach, C.; Albert, M.; Leo, K.; Mikolajick, T. Barrier Performance Optimization of Atomic Layer Deposited Diffusion Barriers for Organic Light Emitting Diodes Using X-Ray Reflectivity Investigations. *Appl. Phys. Lett.* **2013**, *103*, 233302.

(8) Dameron, A. A.; Davidson, S. D.; Burton, B. B.; Carcia, P. F.; McLean, R. S.; George, S. M. Gas Diffusion Barriers on Polymers Using Multilayers Fabricated by Al_2O_3 and Rapid SiO_2 Atomic Layer Deposition. *J. Phys. Chem. C* **2008**, *112*, 4573−4580.

(9) Carcia, P. F.; McLean, R. S.; Li, Z. G.; Reilly, M. H.; Marshall, W. J. Permeability and Corrosion in ZrO_2/Al_2O_3 Nanolaminate and Al_2O_3 Thin Films Grown by Atomic Layer Deposition on Polymers. *J. Vac. Sci. Technol., A* **2012**, *30*, 041515.

(10) Abdulagatov, A. I.; Yan, Y.; Cooper, J. R.; Zhang, Y.; Gibbs, Z. M.; Cavanagh, A. S.; Yang, R. G.; Lee, Y. C.; George, S. M. Al_2O_3 and TiO_2 Atomic Layer Deposition on Copper for Water Corrosion Resistance. *ACS Appl. Mater. Interfaces* **2011**, *3*, 4593−4601.

(11) Kim, N.; Potscavage, W. J.; Domercq, B., Jr.; Kippelen, B.; Graham, S. A Hybrid Encapsulation Method for Organic Electronics. *Appl. Phys. Lett.* **2009**, *94*, 163308.

(12) Klumbies, H.; Müller-Meskamp, L.; Schubert, S.; Moench, T.; Hermenau, M.; Leo, K. Diffusion Barriers for Organic Devices and their Evaluation with Calcium Corrosion Tests. In *Proceedings of the Society of Vacuum Coaters 56th Annual Technical Conference*; Providence, RI, April 20−25, 2013 Society of Vacuum Coaters: Albuquerque, NM, 2013.

DOI: 10.1021/acsami.5b06891
ACS Appl. Mater. Interfaces 2015, 7, 22121−22127

(13) Paetzold, R.; Winnacker, A.; Henseler, D.; Cesari, V.; Heuser, K. Permeation Rate Measurements by Electrical Analysis of Calcium Corrosion. *Rev. Sci. Instrum.* **2003**, *74*, 5147.
(14) Kempe, M. D.; Reese, M. O.; Dameron, A. A. Evaluation of the Sensitivity Limits of Water Vapor Transmission Rate Measurements Using Electrical Calcium Test. *Rev. Sci. Instrum.* **2013**, *84*, 025109.
(15) Schubert, S.; Klumbies, H.; Müller-Meskamp, L.; Leo, K. Electrical Calcium Test for Moisture Barrier Evaluation for Organic Devices. *Rev. Sci. Instrum.* **2011**, *82*, 094101.
(16) Klumbies, H.; Müller-Meskamp, L.; Nehm, F.; Leo, K. Influence of Calcium Corrosion on the Performance of an Adjacent Permeation Barrier. *Rev. Sci. Instrum.* **2014**, *85*, 016104.
(17) Nehm, F.; Dollinger, F.; Klumbies, H.; Leo, K.; Müller-Meskamp, L. Device-like electrical calcium corrosion test for WVTR measurements of ultra-barriers In *Proceedings of the Society of Vacuum Coaters 58th Annual Technical Conference*; Santa Clara, CA, April 27−30, 2015 Society of Vacuum Coaters: Albuquerque, NM, 2015.
(18) Nehm, F.; Müller-Meskamp, L.; Klumbies, H.; Leo, K. Note: Inhibiting Bottleneck Corrosion in Electrical Calcium Tests for Ultra-Barrier Measurements *Rev. Sci. Instrum.*, submitted.
(19) Klumbies, H.; Müller-Meskamp, L.; Mönch, T.; Schubert, S.; Leo, K. The Influence of Laterally Inhomogeneous Corrosion on Electrical and Optical Calcium Moisture Barrier Characterization. *Rev. Sci. Instrum.* **2013**, *84*, 024103.
(20) *Handbook of Chemistry and Physics*, 73rd ed.; Lide, D. R., Ed.; CRC Press:Boca Raton, FL, 1992.
(21) Yue, X.-M.; Zhang, G.-J.; Watanabe, T.; Tai, W.-T. Corrosion Behavior of Single-Crystal Alumina in Argon, Air, and Water Vapor Atmospheres at 1700−2000° C. *J. Am. Ceram. Soc.* **1999**, *82*, 2560−2562.
(22) Groner, M. D.; Fabreguette, F. H.; Elam, J. W.; George, S. M. Low-Temperature Al_2O_3 Atomic Layer Deposition. *Chem. Mater.* **2004**, *16*, 639−645.
(23) van Hemmen, J. L.; Heil, S. B. S.; Klootwijk, J. H.; Roozeboom, F.; Hodson, C. J.; van de Sanden, M. C. M.; Kessels, W. M. M. Plasma and Thermal ALD of Al_2O_3 in a Commercial 200 mm ALD Reactor. *J. Electrochem. Soc.* **2007**, *154*, G165−G169.
(24) Matero, R.; Ritala, M.; Leskelä, M.; Salo, T.; Aromaa, J.; Forsén, O. Atomic layer deposited thin films for corrosion protection. *J. Phys. IV* **1999**, *9*, Pr8−493−Pr8−499.
(25) Bulusu, A.; Kim, H.; Samet, D.; Graham, S., Jr. Improving the Stability of Atomic Layer Deposited Alumina Films in Aqueous Environments with Metal Oxide Capping Layers. *J. Phys. D: Appl. Phys.* **2013**, *46*, 084014.

DOI: 10.1021/acsami.5b06891
ACS Appl. Mater. Interfaces 2015, 7, 22121−22127